We are IntechOpen, the world's leading publisher of Open Access books Built by scientists, for scientists

4,800
Open access books available

122,000
International authors and editors

135M
Downloads

Our authors are among the

154
Countries delivered to

TOP 1%
most cited scientists

12.2%
Contributors from top 500 universities

CLARIVATE ANALYTICS BOOK CITATION INDEX INDEXED

WEB OF SCIENCE™

Selection of our books indexed in the Book Citation Index in Web of Science™ Core Collection (BKCI)

Interested in publishing with us?
Contact book.department@intechopen.com

Numbers displayed above are based on latest data collected.
For more information visit www.intechopen.com

Chapter 3

Perovskite-Based Mesostructures and Related Composites — Influence Exerted by Morphology and Interface

Guilhermina F. Teixeira, Rafael A. Ciola,
Walter K. Sakamoto and Maria A. Zaghete

Additional information is available at the end of the chapter

http://dx.doi.org/10.5772/60654

Abstract

The present work seeks to report about the properties of lead-free $NaNbO_3$ particles with different morphology (cubic-like and fiber-like particles) and their application in composites with poly(vinylidenefluoride) (PVDF) polymer. The composites are obtained using a range of varying volume fractions of $NaNbO_3$ particles (30%, 40%, 50% and 60%). The best conditions for obtaining the $NaNbO_3$ particles as well as the composites have been thoroughly studied. It was observed that the highest volume fraction of $NaNbO_3$ particles undermined the flexibility of the composites. The transition percolation phenomenon, commonly known as percolation threshold, was calculated as a function of the dielectric constant and conductivity of the composite. The composites exhibit piezoelectric and ferroelectric properties and both are found to improve by anisotropy of the NaNbO3 particles.

Keywords: lead-free composites, piezoelectricity, ferroelectricity, anisotropy, percolation threshold

1. Introduction

The ongoing technological developments lead undoubtedly to the quest for anisotropic ceramic material which presents a specific property or a combination of them. To this end, it

is necessary to control the growth parameter of nanostructures controlling the morphology of the particles.

Research on unidimensional nanostructures (1D) arouses multidisciplinary interest owing to their properties which allow the use of these nanostructures in self-assembly devices applicable in optical, electronic, photonic and biological systems [1,2]. Currently, researchers have been trying to develop efficient techniques for obtaining 1D ordered particles in nanoscale, controlling the size and shape of the particles since this is the key to improving the use of existing materials while allowing room for new multifunctional devices.

Ferroelectric and piezoelectric materials are much influenced by structural control, because some materials are found to exhibit piezoelectricity only when they are grown with 1D morphology. Another interesting property of 1D material that is worth mentioning is the photoluminescence (PL). Photoluminescence spectroscopy provides us with important information about electronic and optical structures of the materials such as the intermediate states between the valence band (VB) and the conductive band (CB) known as the band gap [3]. When a material combines the photoluminescence and piezoelectric properties, it can be applicable in piezophotonic devices [4].

Lead zirconate titanate (PZT)-based materials present excellent optical and electronic properties; oddly enough though, despite their good properties, materials like PZT are prone to cause environmental damage which may eventually cause the need for their substitution for lead-free materials.

Alkali niobates, such as sodium niobate ($NaNbO_3$), are promising materials for substituting materials like PZT. $NaNbO_3$ is a lead-free piezoelectric perovskite semiconductor with different phase transitions, which has attracted increasing attention among researchers owing to its capacity to form the basis of the class of environmentally friendly materials [5,6].

The efficiency of these materials is said to be directly related to their crystalline and morphological structures. One possibility of obtaining particles with crystalline and morphological well-defined characteristics lies in hydrothermal synthesis, which is a variation of solvothermal synthesis.

The heating in hydrothermal synthesis can be carried out by microwave-assisted technique and when this happens the synthesis is named microwave hydrothermal synthesis. This process, in particular, is truly a low-temperature method for the preparation of monophasic materials of different sizes and shapes. This method is found to save energy and is environmentally friendly in that the reactions take place in closed system conditions. Unlike the conventional heating which requires a long time of reaction, microwave-assisted heating is a greener approach toward the synthesis of materials in a shorter time (several minutes to hours) with lower power consumption as a result of the direct and uniform heating of the contents [7].

Although some ceramics are known to have high ferroelectric and piezoelectric properties, their poor mechanical properties and other properties including the mismatch of the acoustic impedance with water and human tissue are found to restrict their application. On the other hand, ferroelectric polymers possess excellent mechanical properties such as flexibility and

http://dx.doi.org/10.5772/60654

deformation, but their piezoelectric activity is low. To circumvent these problems, composite materials made with ferroelectric ceramic and polymer have been investigated as an alternative material which combines the electric properties of ceramic and mechanical properties of polymer [8].

A core parameter to be considered when discussing about composites lies in the connectivity patterns, which establish the arrangement of the phases comprising the composites. The first concept of connectivity was developed by Skinner et al [9] and Newnham et al [10], where the manner in which the individual phases are self-connected are described. There are 10 types of arrangements in which the two components, the matrix phase and the dispersed phase, can be connected forming the composite, ranging from unconnected 0-3 pattern to a 3-3 pattern in which both phases are three-dimensionally self-connected. The first number in the notation represents the dimension of connectivity for the piezoelectric active phase, while the second number refers to the electromechanically inactive polymer phase [11,12]. The composites with 0-3 connectivity possess the merits of being highly flexible and having a relatively high piezoelectric coefficient, though it is very difficult to obtain 0-3 composites with a high ceramic content. The high ceramic content provides a mixed connectivity in 0-3 composites due to the percolation of the particles, besides that the high concentration of big ceramic particles is found to reduce the flexibility of the composite [8]. The 3-3 composites when compared with the 0-3 composites are found to present a relatively higher piezoelectric coefficient [12] though they are quite more rigid and difficult to manufacture than the latter (0-3). Studies conducted on lead-free composites using KNN particles (sodium potassium niobate) and poly(vinylidene-fluoride) (PVDF) as polymer concluded that the piezoelectric activity tends to increase given an increase in the ceramic content. However, a decrease in the polymeric phase of the composite weakens the mechanical properties. The piezoelectric properties of the KNN/PVDF composite were compatible with the PZT-based materials, implying that it is a good option to be used in place of PZT-based materials [13].

A wide array of studies on piezoelectric composites can be found in the literature. Dargahi et al [14] developed a composite to be used in the medical area as a sensor in minimally invasive surgeries without damage to the body. Fuzari Jr et al [15] studied a promising material to use as an acoustic emission sensor. A $NaNbO_3$/PVDF composite used in energy harvest was obtained by Mendoza et al. and Srinivas [16,17], where they compared the $NaNbO_3$/PVDF and lead-based ceramic/PVDF composite in order to demonstrate the feasibility of replacing lead-containing materials in high-energy-density dielectric capacitors.

Despite the range of advantages attributable to composite materials, the poling process still poses a challenge owing to the fact that the effective electric field for polarizing the ceramic particles is much lower compared to the applied electric field [15,18,19]. The poling efficiency of ceramic particles dispersed in a polymer can be enhanced inserting a third phase into the composite. This phase creates an electrical flux path between the ceramics particles, and to promote this effect a conducting polymer, polyaniline (PAni), for instance, can be included in the composite to control the electrical conductivity [15].

In light of that, the main purpose of this study is to discuss the preparation and characterization of $NaNbO_3$ ceramic particles with different morphology obtained by microwave-assisted

hydrothermal synthesis. The influence exerted by the synthesis parameter in obtaining the particles with the best characteristics as well as the use of these particles in the fabrication of composite films with 0-3 connectivity, using PVDF as polymer matrix, are all presented and discussed.

2. Experimental processing

2.1. $NaNbO_3$ synthesis

$NaNbO_3$ powders were obtained by microwave hydrothermal synthesis which was carried out beginning with NaOH (p. a. Quemis) and Nb_2O_5 (Alfa Aesar, 99%). In the reaction to form $NaNbO_3$, the NaOH acts as a mineralizing agent and sodium source. The reaction was carried out in a Teflon vessel model XP-1500 (CEM Corp.), in a MARS-5 (CEM Corp.) microwave oven. The precursor suspensions were prepared with 0.696 g of Nb_2O_5 added to 30 mL of 8 $mol.L^{-1}$ NaOH water solution. The suspension was then transferred into Teflon vessels which were placed inside a microwave furnace. The synthesis was carried out at 180°C with different conditions as given in Table 1. The obtained powders were thoroughly washed with distilled water by centrifugation and finally dried at room temperature.

Microwave Power (W)	Synthesis Time (minutes)
300	30
	60
	120
	180
	240
600	30
	60
800	30
1000	30

Table 1. Microwave hydrothermal synthesis conditions for obtaining $NaNbO_3$ particles.

2.2. Reaction Mechanism to form $Na_2Nb_2O_6.H_2O$ and $NaNbO_3$

The NbO_7 decahedra and NbO_6 octahedra resulted from the breaking up of the Nb_2O_5. The NbO_7 and NbO_6 are connected by corner forming $Nb_6O_{19}^{8-}$ hexaniobate *Lindqvist* ion, which can provide different niobate compositions. These compositions are related to the different synthesis conditions used to obtain the materials.

In solution, the $Nb_6O_{19}^{8-}$ ions incorporate Na^+ ions forming $Na_2Nb_2O_6.nH_2O$ microfibers, followed by structural rearrangement, releasing water molecules forming $NaNbO_3$ structures [20,21,22].

http://dx.doi.org/10.5772/60654

The reaction mechanism between Nb_2O_5 and NaOH to form $NaNbO_3$ can be described by the equations below:

$$3\ Nb_2O_5 + 8\ OH^- \rightarrow Nb_6O_{19}^{8-} + 4\ H_2O \quad (1)$$

$$Nb_6O_{19}^{8-} + 34\ OH^- \rightarrow 6\ NbO_6^{7-} + 17\ H_2O \quad (2)$$

$$2\ NbO_6^{7-} + 2\ Na^+ + 7\ H_2O \rightarrow Na_2Nb_2O_6.H_2O + 12\ OH^- \quad (3)$$

$$Na_2Nb_2O_6.H_2O \rightarrow 2\ NaNbO_3 + H_2O \quad (4)$$

2.3. $NaNbO_3$ particles characterization

The obtained powders were characterized by X-ray powder diffraction using a rotatory anode diffractometer (Rigaku-RINT 2000) with divergent cleft of 0.25°, soller cleft of 2.5° of divergence in the 2θ range from 20° to 80° with 0.2 graus.min^{-1}. The morphology of as-prepared samples was observed using a high-resolution field-emission gun scanning electron microscopy FE-SEM (GERMA JEOL JSM 7500F Field Emission Scanning Electron Microscopy). PL spectra were collected with a Thermal Jarrel-Ash Monospec 27 monochromator and a Hamamatsu R446 photomultiplier. The 350 nm exciting wavelength of a krypton ion laser (Coherent Innova) was used with the nominal output power of the laser kept at 550 mW. All measurements were performed at room temperature.

Figure 1 shows the diffraction powder patterns of X-ray obtained for the powder synthesis carried out at 300 W. Based on the results, it is observed that a pure orthorhombic crystalline structure of $NaNbO_3$ is favored by a rise in the synthesis time period, which is in accordance with the JCPDS file nº 33.1270. For the 30 and 60 minute synthesis times, the obtained product consisted of $Na_2Nb_2O_6.nH_2O$. When the synthesis times are increased to 120 and 180 minutes, the products are a mixture of $Na_2Nb_2O_6.nH_2O$ and orthorhombic $NaNbO_3$ and a diffractogram peak attesting to the decreasing of $Na_2Nb_2O_6.nH_2O$ until it disappears following 240 minutes of synthesis indicating the formation of orthorhombic $NaNbO_3$ pure phase.

The presence of microwave enables the obtaining of $NaNbO_3$ crystalline phase in a short synthesis time and this time can be even smaller when the power of microwave is increased. Figure 2 shows the X-ray diffraction of products obtained using a higher power above 300 W. Using 600 W for 30 minutes, peaks related to $Na_2Nb_2O_6.nH_2O$ were observed and a pure orthorhombic $NaNbO_3$ was seen using 600 W for 60 minutes. By increasing the power to 800 or 1000 W, it is worth noting that the time for obtaining the orthorhombic $NaNbO_3$ pure phase was found to decrease to 30 minutes.

According to Zhu et al [21], $Na_2Nb_2O_6.nH_2O$ is a microporous metastable phase with fiber morphology resulting from $NaNbO_3$ crystallization. The $Na_2Nb_2O_6.nH_2O$ phase presents monoclinic crystalline structure belonging to the C2/*c* space group with lattice parameters *a* = 17.0511 Å, *b* = 5.0293 Å, *c* = 16.4921 Å e β=113.942 Å and are applied in SOMS, Sandia Octahedral Molecular Sieves [20]. The dehydration of $Na_2Nb_2O_6.nH_2O$ promotes the formation of $NaNbO_3$ perovskite phase which is energetically more stable [20].

Under hydrothermal conditions, $NaNbO_3$ formation occurs as a result of the dissolution of Nb_2O_5 in NaOH environment, which is favored by the rise in synthesis time. While the Nb_2O_5 is dissolved, OH^- ions are adsorbed on the Nb_2O_5 surface, thereby promoting the affinity between Nb=O and O-H bonds forming Nb=O···OH···O=Nb [23].

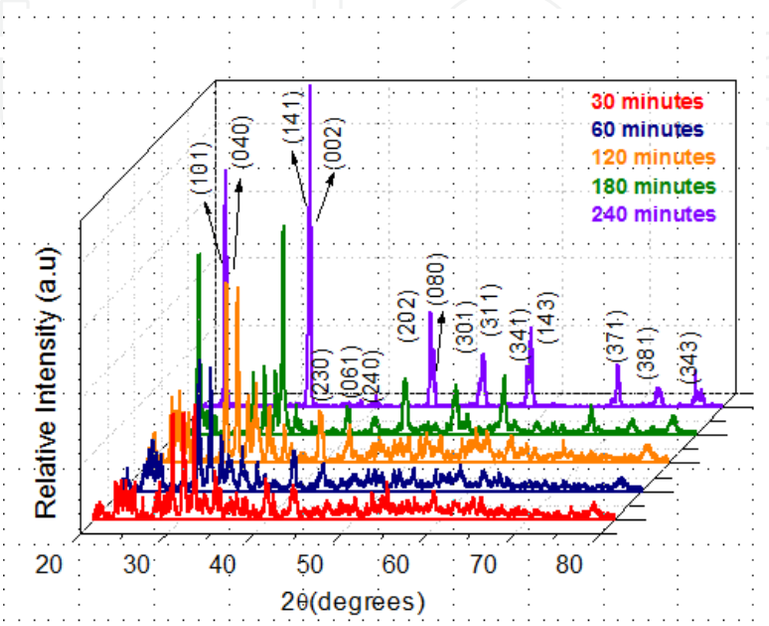

Figure 1. XRD patterns of particles obtained by microwave hydrothermal synthesis using 300 W at 180°C in different synthesis time.

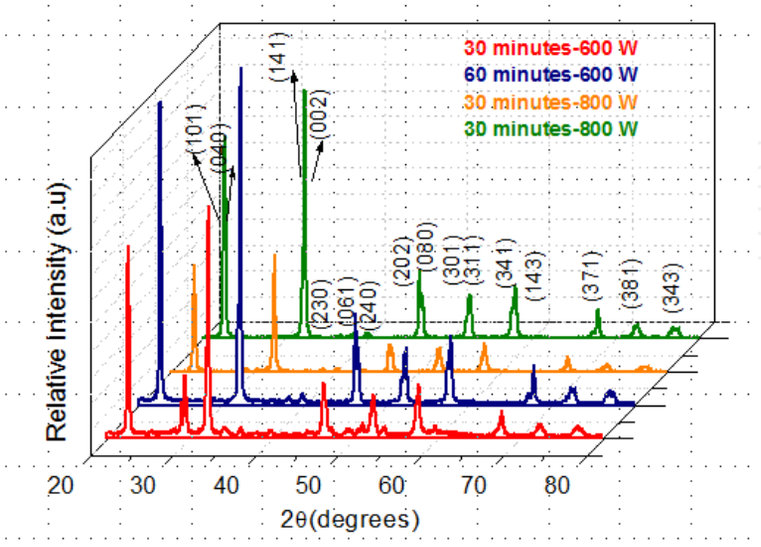

Figure 2. XRD patterns of particles obtained by microwave hydrothermal synthesis using 600 W, 800 W and 1000 W at 180°C.

http://dx.doi.org/10.5772/60654

The morphological changes regarding the process are shown in Figure 3, where one can observe that the products presented different morphologies. It is noteworthy that for the 30 and 60 minutes synthesis times with 300 W of power, the samples were composed of $Na_2Nb_2O_6.nH_2O$ structures with fiber-like shape (Figures 3 A–B). For the 120 and 180 minutes synthesis times, there is a mix of fiber and plate-like structures (Figure 3C), and when the synthesis time is increased to 240 minutes, only particles with cube-like morphology are observed (Figure 3D). These results confirm the XRD results (Figure 1) as it is possible to observe that given an increase in the synthesis time, the fiber morphology corresponds to the $Na_2Nb_2O_6.nH_2O$ until the formation of orthorhombic $NaNbO_3$ with a cubic shape [24,25].

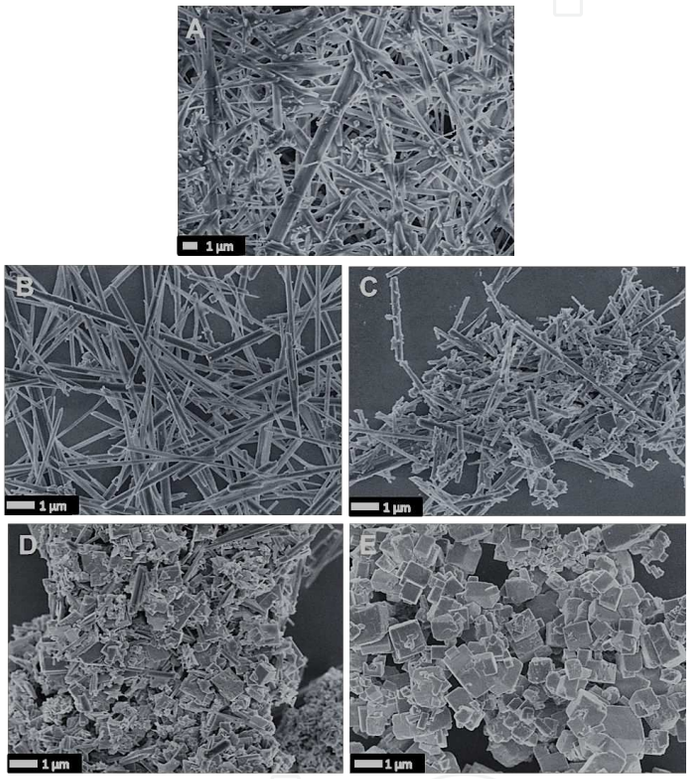

Figure 3. FE–SEM of particles obtained by microwave hydrothermal synthesis at 300 W. (A) 30 minutes; (B) 60 minutes; (C) 120 minutes; (D) 180 minutes; (E) 240 minutes.

Using 600 W power, the particles obtained in the shortest time – 30 minutes – also presented fiber morphology, while presenting a cubic morphology after 60 minutes of synthesis (Figure 4 A–B). By increasing the power, the time to obtain the $NaNbO_3$ cubic morphology decreases to 30 minutes, though the particles are clustered as can be seen in Figure 4 C–D.

The morphological evolution of $NaNbO_3$ obtained by hydrothermal synthesis was extensively studied by Zhu et al [21]. NaOH breaks the octahedra corner sharing formed by Nb–O from Nb_2O_5 forming intermediaries octahedral edge sharing, which presents low crystallinity. The dissolution of intermediate gives NbO_6 which promotes the growth of metastable compound with fiber shape. Finally, increasing the synthesis time, the fibers are dissolved and the NbO_6 octahedral takes the form of $NaNbO_3$ with a cubic shape.

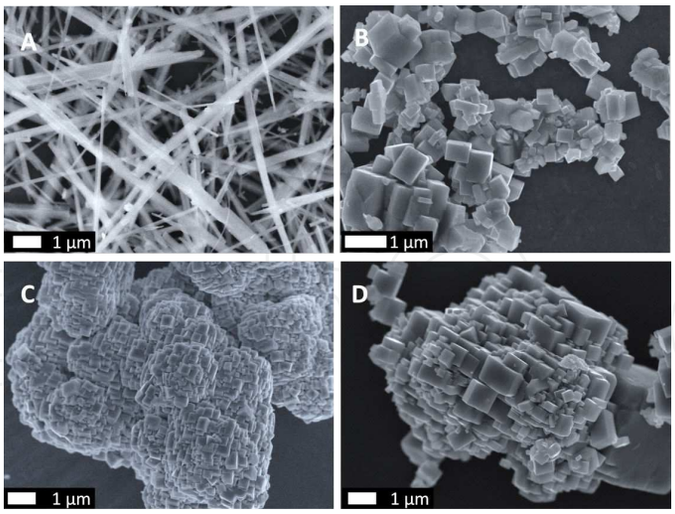

Figure 4. FE–SEM of particles obtained by microwave hydrothermal synthesis using different powers.(A) 30 minutes and 600 W; (B) 60 minutes and 600 W; (C) 30 minutes and 800 W; (D) 30 minutes and 1000 W.

By means of the conventional hydrothermal synthesis using the Pluronic P123 copolymer (EO20PO70EO20, BASF, USA), Shi et al [26] obtained orthorhombic $NaNbO_3$ with a fiber shape. The copolymer assists the particles crystallization during the reaction between Nb_2O_5 and NaOH at 200°C for 24 hours. Replacing the P123 with PEG-1000 (polyethylene glycol), cubic-like particles with a narrow size distribution is obtained. Ke et al [27] report the change of $NaNbO_3$ morphology in line with the NaOH concentration used in the synthesis. The materials obtained from $NaNbO_3$ with 1D morphology including fibers and wires can present good piezoelectric property [4]. A process used to obtain this morphology is the thermal treatment of $Na_2Nb_2O_5.H_2O$ at temperatures around 300–550° C. The thermal treatment changes the crystalline structure of the material maintaining the 1D shape. Although piezoelectricity is an anisotropic property, the $NaNbO_3$ with cubic morphology hardly presents good piezoelectricity due to the high symmetry of the cubes.

In this work, the thermal treatment of the product was carried out for a period of 4 hours at 550°C by microwave hydrothermal synthesis with 300 W at 180°C for 30 minutes; the metastable phase of $Na_2Nb_2O_5.nH_2O$ is transformed into the orthorhombic structure of $NaNbO_3$ maintaining the fiber-like morphology as shown in Figure 5. The thermal treatment promotes the dehydration of $Na_2Nb_2O_6.nH_2O$, forming $NaNbO_3$ perovskite phase, which is found to be energetically more stable than $Na_2Nb_2O_6.nH_2O$.

In a previous work, we reported about the PL properties at room temperature of $NaNbO_3$ particles and film as a function of anisotropic morphology; the $NaNbO_3$ particles in question are fiber and cubic-like morphologically structured, being that the fibers are originated from the thermal treatment of $Na_2Nb_2O_6.nH_2O$ fibers. The particles which presented major PL intensity are $Na_2Nb_2O_6.nH_2O$ fibers prior to thermal treatment, and the smaller PL emission is found to be presented by $NaNbO_3$ fiber-like particles [22].

The order–disorder of the materials including surface defects, cation or anion vacancies, lattice distortions and the recombination process in semiconductors can be evaluated based on the

http://dx.doi.org/10.5772/60654

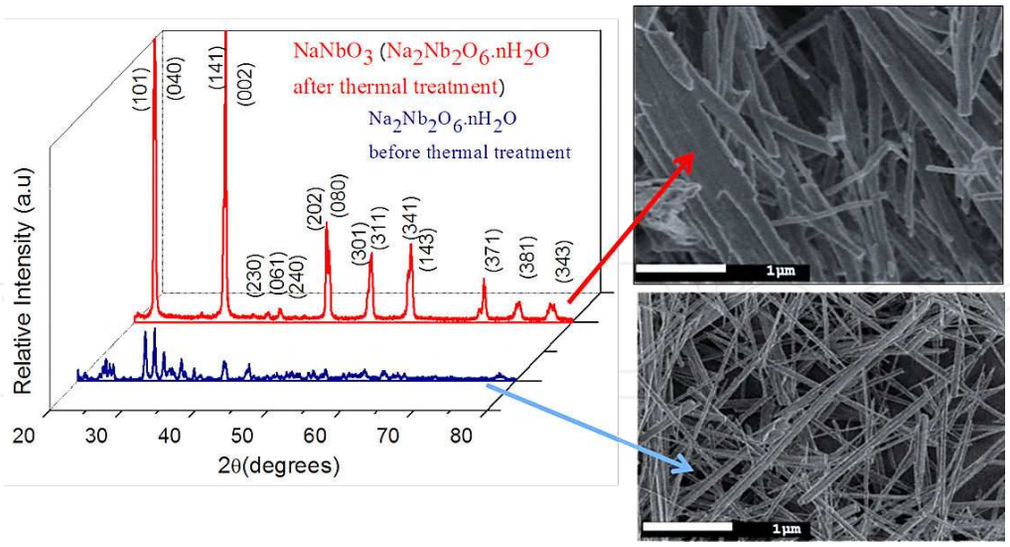

Figure 5. XRD patterns and FE–SEM of $Na_2Nb_2O_5.nH_2O$ prior to following thermal treatment at 500°C for 4 hours to form $NaNbO_3$ particles.

PL process. PL is an efficient method for investigating the electronic structure and optical properties of materials. PL properties are a great probe for investigating changes around the site environment at short-range (2–5 Å) and medium-range order (5–20 Å) of clusters where the degree of local order is pronounced [28]. The PL emission region is associated to the defects of the materials. When the material presents deep-level defects, it generates intermediary energy levels near the conduction band which are represented by the PL emission at low energy (yellow/green region of electromagnetic spectrum). Shallow levels generate states next to the valence band where they exhibit PL emission at a higher energy (violet/blue region) [28].

Prior to thermal treatment, the fibers show PL emission around 550 nm, which is then found to decrease following thermal treatment. Furthermore, the band is seen to shift toward a higher energy region. Like the $NaNbO_3$ fiber, the cubic particles also emit higher energy (450 nm) (cf. Figure 4 Ref 22), and this displacement indicates that $NaNbO_3$ crystalline structure is more stable compared to $Na_2Nb_2O_6.nH_2O$ [22].

At low temperature, Almeida et al [29] obtained two PL bands centered at approximately 430 nm and 540 nm in glass-ceramic-containing $NaNbO_3$ crystal. The emission at 430 nm was attributed to the direct exciton recombination, and the low quantum efficiency is likely to indicate that the emission at 540 nm emanates from trap states. At room temperature, the PL band is centered only in the region around 430 nm, next to $NaNbO_3$ PL emission region as we have reported in a previous work [22].

In a previously published paper [22], we proposed that the PL bands can be attributed to the bulk energy levels consistent with their attribution to the transitions between O^{2-} and Nb^{5+}, based on the local structure of NbO_6 octahedra. By similar structure analyses, NbO_6 assumes the form of a regular octahedron, which comes from the strong covalent bonding as a result of the orbital hybridization between Nb **d** and O **2p**. Without the presence of structural defects capable of changing the clusters organization, this crystalline structure is characterized by a

high symmetry. However, the order–disordered $NaNbO_3$ presents a symmetry rupture along the O–Nb–O bonds that result in complex clusters with different coordination numbers ($[NbO_6]$–$[NbO_5]$) or distortions in the $[NbO_6]$–$[NbO_6]$ octahedral clusters. The wide-band visible emission observed is a characteristic property of practically all self-activated ABO_3 perovskites [22,30].

Some materials present a change in the PL emission according to the morphology [31]. However, as far as our investigation is concerned, the PL results are seen not to be related to the morphology of the $NaNbO_3$ but rather to the organization of the crystalline structure. This observation is backed by the results observed in [22] where the orthorhombic $NaNbO_3$ presents fiber-like and cubic-like particles, where both have PL emission in the same region. The PL emission region observed here is not the same for $Na_2Nb_2O_6.nH_2O$ which presents fiber-like particles to boot [22].

The microwave hydrothermal process is capable of producing $NaNbO_3$ with a more disorganized structure when compared to $NaNbO_3$ obtained by thermal treatment of $Na_2Nb_2O_6.nH_2O$. This can be associated to the heating of $Na_2Nb_2O_6.nH_2O$ so as to yield $NaNbO_3$ with fiber-like morphology which tends to promote a better self-assembly of the crystalline structure than in cubic-like particles. This assembly decreases the structural defects as well as the intermediary levels within the band gap, resulting in a lower PL emission [22].

3. Composite processing

3.1. Polymer matrix: PVDF

PVDF is a piezoelectric polymer (d_{33}= –33 pC/N) that is able to produce variation in the surface charge when subjected to mechanical stress without requiring additional energy sources or electrodes for the generation of electrical signal. This polymer consists of a carbon-based chain with alternating hydrogen and fluorine units (–CH_2–CF_2–)n, and its molecular weight is around 105 g.mol^{-1}. PVDF presents polymorphism and can be found in four structural phases (α, β, γ and δ) where the piezoelectric phase is said to be the β phase once it is a polar phase [8,32].

3.2. Obtaining $NaNbO_3$ 1D nanostructures modified by polyaniline (PAni)

PAni (polyaniline) is a conducting polymer in which the electrical conductivity can be modified by the protonation process controlling the reaction pH [15], and its use to cover ceramic particles has the ability to improve the conductivity of particles.

To obtain PAni, the monomer aniline ($C_6H_5NH_2$) (Sigma-Aldrich) was used after vacuum distillation to remove photoxidized molecules. The oxidant ammonium persulfate was employed for the polymerization process of aniline (MERCK).

To obtain $NaNbO_3$ fiber particles coated with PAni, the fibers were incorporated into a solution of aniline, cloridric acid water solution, 1 mol.L^{-1}, and ammonium persulfate under stirring at

http://dx.doi.org/10.5772/60654

temperature around 2°C for approximately 1 hour. This suspension displayed a green color, a feature of protonated PAni (conductive). The deprotonation process was performed by washing the green particles with ammonium hydroxide water solution, 0.1 $mol.L^{-1}$; in this condition the particles presented a blue color (not conductive). Finally, the particles were protonated again through the use of a solution with pH = 3.7 containing cloridric acid (1 $mol.L^{-1}$) and ammonium hydroxide (0.1 $mol.L^{-1}$). At the end of the process, the particles displayed a green color again (conductivity controlled).

Observing the FE–SEM image depicted in Figure 6, it is possible to note that the covering did not change the morphology of the particles.

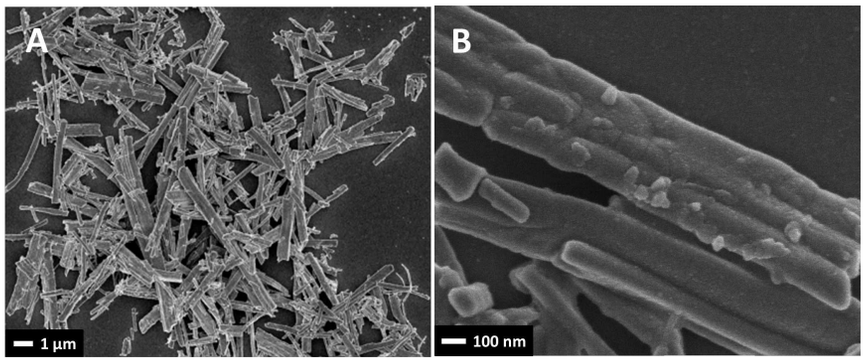

Figure 6. FE–SEM image of (A) $NaNbO_3$ fiber-like particles covered with reprotonated PAni and (B) larger image.

3.3. Fabrication of composite

α-PVDF in powder form was mixed in a mortar with pure $NaNbO_3$ particles with both morphologies (fiber and cubic particles). In addition, the $NaNbO_3$ fiber-like particles coated with PAni were mixed in a mortar with PVDF until a homogeneous mixture was formed. The mixtures were then placed between sheets of Kapton and hot pressed at 190°C for 5 minutes with a pressure of 5 MPa. The thickness of the films is in the range of 190 to 500 µm depending on the ratio of ceramic/polymer content. The composite films from pure $NaNbO_3$ particles were obtained with volumetric fractions of ceramic (30%, 40%, 50% and 60%), while those from $NaNbO_3$ fibers modified with PAni were obtained with 30% and 40% of volume fraction of ceramic. The composites obtained from fiber-like particles without PAni will be denoted by FbNN while the particles coated with PAni will be denoted by PbNN-$PAni_{rep}$, and composites from cubic-like particles will be represented by CbNN.

The volume fraction of ceramic was calculated using the equation 5 [8,33].

$$m_c = \frac{m_p \rho_c}{\rho_p} \frac{\Phi_c}{1 - \Phi_c} \tag{5}$$

In the equation m is the mass and ρ is the density. The subscript c and p are related to ceramic and polymer, respectively. Φ_c is the volume fraction of ceramic.

Figure 7, 8 and 9 show the FE–SEM images of the composite sample. The distribution of the ceramic particles in the polymer matrix likewise the difference between the samples surface according to the increase in the ceramic particles can be observed. The inhomogeneity of the sample with 60% of ceramic particles led to the lowest flexibility of the composite owing to the high concentration of particles and the change in connectivity.

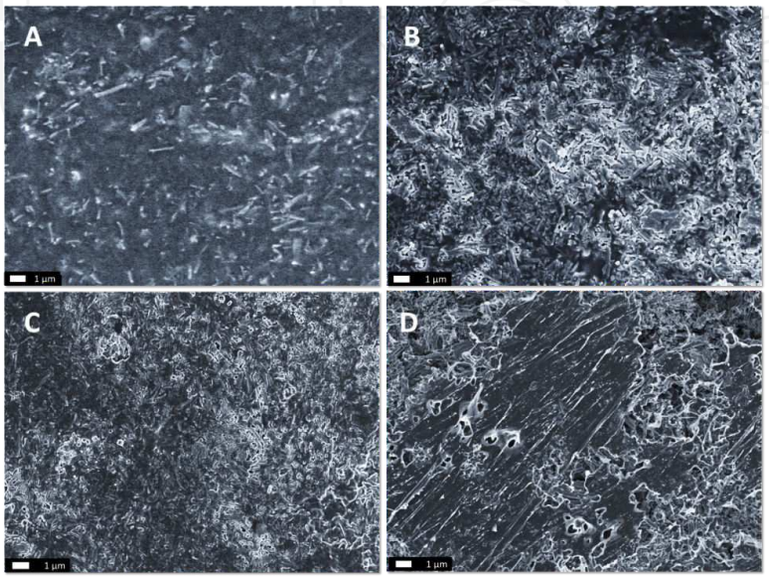

Figure 7. FE–SEM of surface of FbNN composites with the respective volume fraction of $NaNbO_3$ particles: (A) 30%; (B) 40%; (C) 50%; (D) 60%.

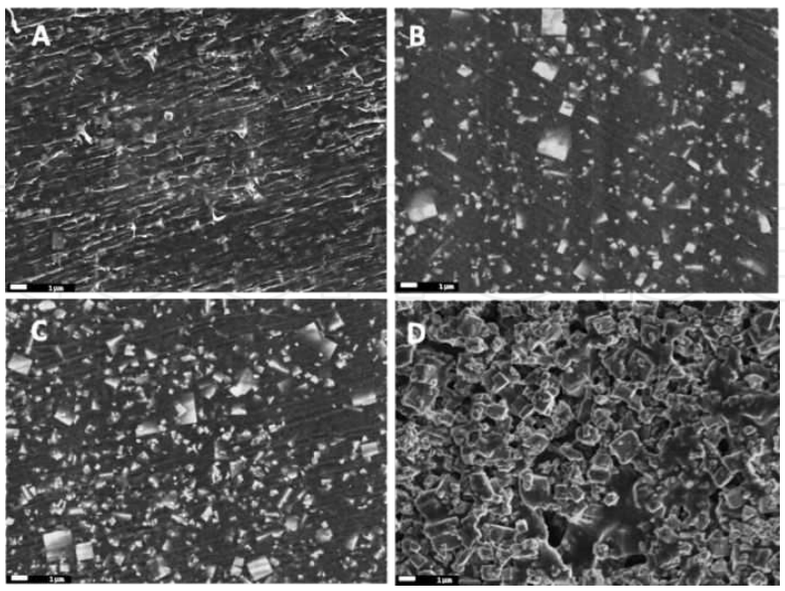

Figure 8. FE–SEM of surface of CbNN composites with the respective volume fraction of $NaNbO_3$ particles: (A) 30%; (B) 40%; (C) 50%; (D) 60%.

http://dx.doi.org/10.5772/60654

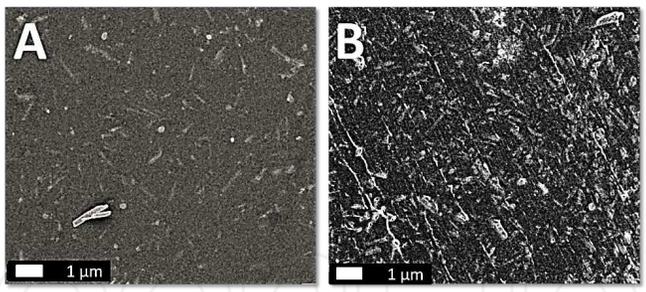

Figure 9. FE–SEM of surface of FbNN–PAni$_{rep}$ composites with the respective volume fraction of $NaNbO_3$ particles of: (A) 30%; (B) 40%.

3.4. Composite characterization

To carry out the electric measurements, a contact was deposited onto both sides of the samples; gold electrodes with 1.0 cm of diameter were vacuum evaporated. The composite films were poled with an electric field of 5 MV/m at 90°C during 60 minutes in silicone oil.

A TREK high-voltage power supply was used for the poling process. By measuring the longitudinal piezoelectric coefficient d_{33}, the piezoelectric activity of the composite was studied. In order to acquire the longitudinal piezoelectric coefficient d_{33} Pennebaker Model 8000Piezo d_{33} Tester was used (American Piezo Ceramics Inc) coupled to a multimeter 34401A (Hewlett Packard).

To avoid problems with lack of uniformity of the composites, the measurements were made at least in 10 different points for each sample, where the average value of these points was taken as the coefficient d_{33}.The sample with 50% and 60% of ceramic particles could not be poled because it got ruptured during the polarization process due to the high electric field applied. The improvement in the piezoelectric coefficient is proportional to the anisotropy of the $NaNbO_3$ particles and the volumetric ratio of the ceramic particles was found to scatter in the polymeric matrix. The values of d_{33} obtained for the composites containing $NaNbO_3$ particles are listed in Table 2.

Sample	Volumetric fraction of ceramic (%)	*d33* (pC/N)
FbNN	30	2.5
FbNN	40	7.8
CbNN	30	0.9
CbNN	40	1.1
FbNN–PAni$_{rep}$	30	5.7
FbNN–PAni$_{rep}$	40	9.0

Table 2. The values of d_{33} found for the composite with $NaNbO_3$ obtained in different conditions.

Table 3 shows the values of d_{33} piezoelectric constant for some ceramic/polymer composites. It is possible to observe that for the lowest volumetric ratio of ceramic in the composites, the piezoelectric response for the composite with the ceramic particle covered with PAni (FbNN–PAni rep/PVDF composite) was found to be better than almost all the composites with the same volumetric fraction of ceramic. This value is only smaller than that of PZT/PAni/PVDF composite.

Composites	Volumetric fraction of ceramic (%)	*d33* (pC/N)
PZT/PHB [34]	30	1.0 to ~3.2*
PZT/PHB [34]	30	~1.0 to 4.0**
PZT/PAni/PVDF [15]	30	16
PZT/PVDF [35]	30	4.5
BT/PVDF [36]	30	4.2
BT/PVDF [36]	50	5.5

*Sample poled at different temperatures; **Sample in different electric field

Table 3. The values of d_{33} found for some composites in the literature.

Malmonge et al verified the increase in d_{33} as a consequence of the increase in temperature and electric field used for the poled PHB–PZT composite (PHB = poly-β-hydroxybutyrate), indicating the possible application of the composite in areas related to sensors [34].

Hysteresis loop provides information about the remnant polarization (P_r) of the composites. The P*r* values were obtained using a Radiant Technologies Inc RT 6000 HVS High Voltage Test System. The measurements were carried out at room temperature using varying electric fields (100 and 600 V) and frequencies (2.5 Hz, 5 Hz, 20 Hz and 40 Hz). The FbNN and CbNN (containing 30% and 60% volumetric fraction of ceramic) and FbNN–PAni$_{rep}$ with 30% are graphically represented by hysteresis loop, Figures 10, 11 and 12.

The increase in voltage applied provides higher values of electric field; and for the samples with a greater thickness, the electric field value is found to decrease. The increase observed in the P_r is proportional to the increase of voltage applied and to the decrease in frequency. Low frequency promotes the increasing of P_r value and the rounding of hysteresis loop to the same conditions. This happens as a result of the longer cycle times and the longer relaxation time for different charge carriers and dipoles. This can be explained by the fact that some charges are able to follow the electric field whereas other charges are not. There are charges that need longer relaxation time. The increase in the volumetric fraction of the ceramic leads to a higher P_r value, though with the demerit of having a lower flexibility of composite. In the FbNN–PAni$_{rep}$, the presence of a conducting polymer is found to improve the P_r value. Another factor that improves the P_r value is the anisotropy of the particles because it is possible to observe that for the FbNN composites all the P_r values are better than the ones for the CbNN composites.

http://dx.doi.org/10.5772/60654

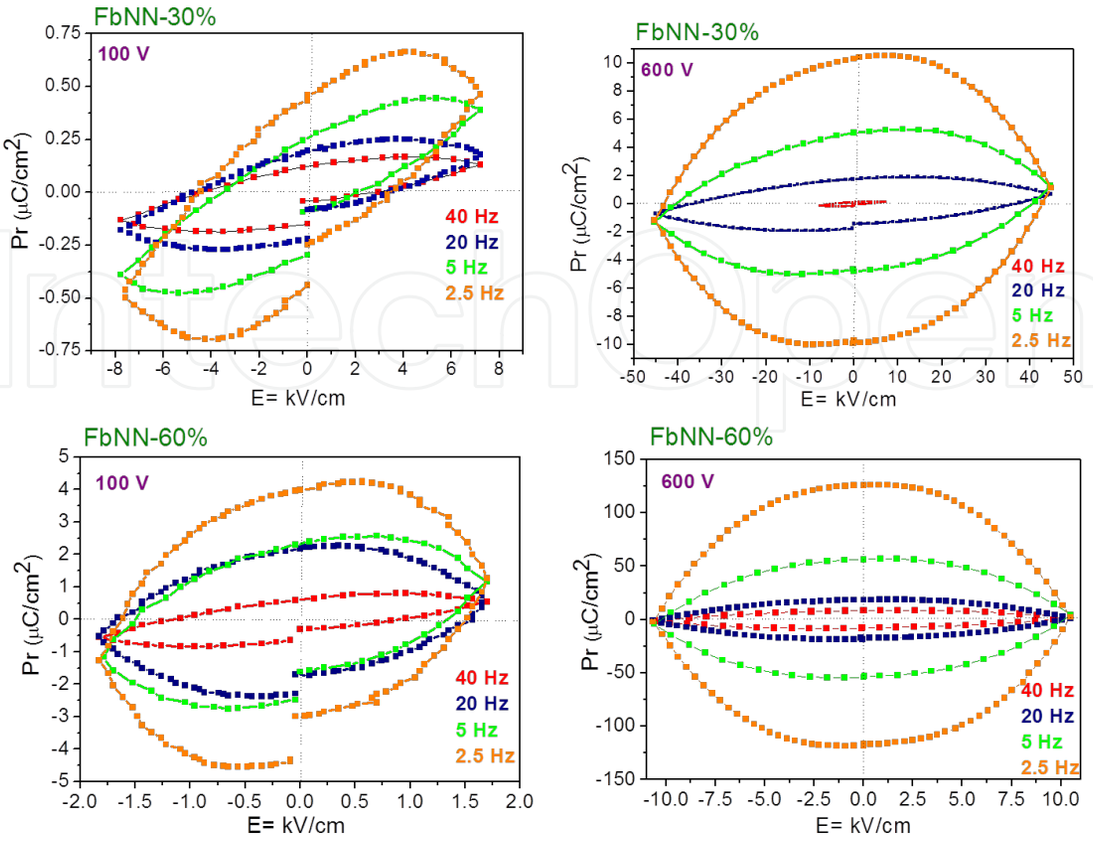

Figure 10. *P-E* loops for FbNN composites. (Applied voltage: 100 and 600 V)

The solid materials are classified according to their ease of conducting electrical current. When they have low conductivity in the range of 10^{-14} to 10^{-10} Ω-m, they are classified as insulators; semiconductors have conductivity between 10^{-9} and 10^{-1} Ω-m; besides, a conductive material has conductivity higher than 10^{2} Ω-m [37].

The characterization of composite materials indicates that conductivity is of essential relevance owing to the fact that there are multimodal microstructures and each phase has intrinsic properties which determine the properties as well as the applications of the composite.

Considering that the union of the different phases occurs only by physical contact of the surfaces, known as interfaces, no chemical bond formation is observed. Therefore, the layers that form the composite (matrix/disperse phase) can be said to retain their distinct conductivity.

The heterogeneity of microstructure consists of single phase regions which are statistically distributed in the volume of composite, and the macroscopic properties of the composite that are directly connected to this distribution [38]. In the composite preparation method and in the volumetric fraction of each phase there are parameters which directly influence the resulting properties. The influence of each phase in the composite characteristics is associated with the intrinsic characteristics. The volume fraction of the disperse phase (one perovskite oxide) and the composites matrix which is an insulating polymer, is dependent on the

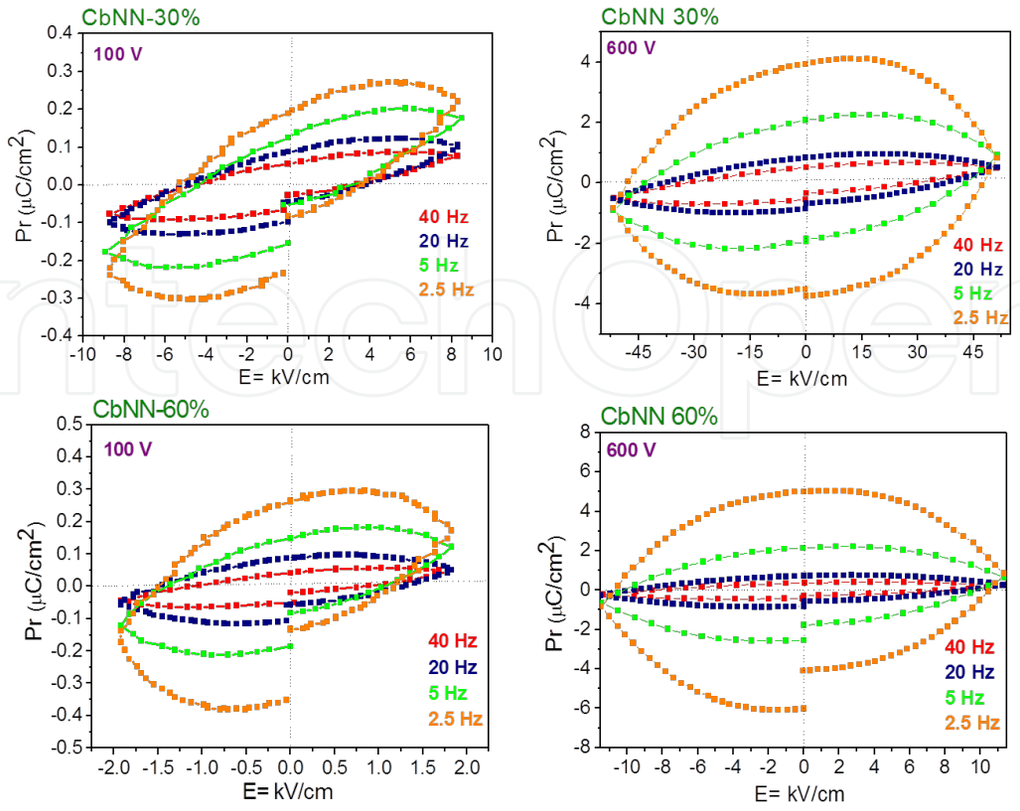

Figure 11. *P-E* loops for CbNN composites. (Applied voltage: 100 and 600 V)

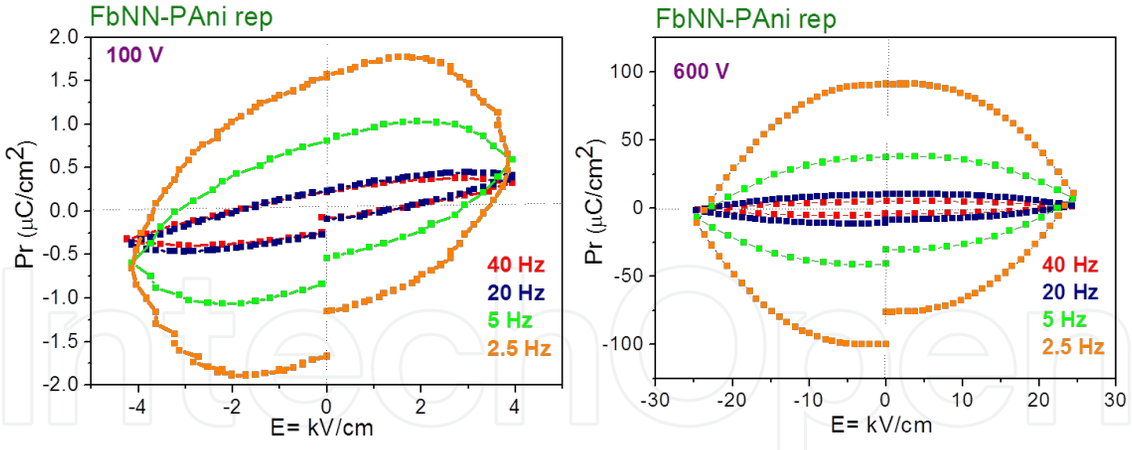

Figure 12. *P-E* loops for FbNN–PAni$_{rep}$ composite. (Applied voltage: 100 and 600 V)

embedded oxide fraction in the polymer matrix. Depending on the process, it can be isolated or connected to the polymer. The percolation transition phenomenon, commonly known as the percolation threshold, occurs during the transition from the isolated oxide behavior to the interconnected oxide behavior. The percolation threshold is a mathematical term related to the percolation theory which involves long-range bond formation in a random system. Below the limit, the component or system as a whole is not connected, and over the limit there is a

http://dx.doi.org/10.5772/60654

greatness component that is bigger than the system itself and which exerts influence on the overall behavior of the composite. The presence of a metal as a dispersed phase in the polymer matrix paves the way for the occurrence of an insulator/conductor interface transition [39].

Close to the percolation threshold, the value of the electrical conductivity and the dielectric constant of the composite increases abruptly in several orders of magnitude. However, the composite type insulator/semiconductor presents a remarkable increase in the dielectric constant with high values and a relatively low conductivity range, close to the percolation threshold [40].

The actual conductivity of the material is directly proportional to the interaction between the dispersed phase and the matrix phase expressed through the power law (a functional relationship between two quantities, where one varies as potency of the other). Mathematically, the effective conductivity (σ) or the effective dielectric constant (ε) of the composite is described by the following equations [38,40].

$$\sigma_{eff} = \sigma_f \left(f_f - f_c \right)^t, \text{ to } f_f > f_c \tag{6}$$

$$\sigma_{eff} = \sigma_{PVDF} \left(f_c - f_f \right)^{-s}, \text{ to } f_f < f_c \tag{7}$$

$$\varepsilon_{eff} = \varepsilon_f \left(f_f - f_c \right)^{t'}, \text{ to } f_f > f_c \tag{8}$$

$$\varepsilon_{eff} = \varepsilon_{PVDF} \left(f_c - f_f \right)^{-s'}, \text{ to } f_f < f_c \tag{9}$$

where $\mathbf{f_f}$ is the fraction of the disperse phase; $\mathbf{f_c}$ is the percolation threshold; $\boldsymbol{\sigma_f}$ the conductivity of the dispersed phase; $\boldsymbol{\sigma_{PVDF}}$ and phase conductivity matrix (PVDF); $\boldsymbol{\varepsilon_f}$ the dielectric constant of the disperse phase and $\boldsymbol{\varepsilon_{PVDF}}$ the dielectric constant of the matrix phase. The **t** e **s** exponents are the critical values of the conductive region and the insulating region. Some articles that have already been published reported that the percolation threshold is influenced by the size, morphology and constitution of particles that form the dispersed phase [41,42]. The composites analyzed in this study consist of PVDF, as polymer matrix phase and $NaNbO_3$ as dispersed phase. The chemical composition and crystal structure of the dispersed phase are fixed, though we have two distinct particle morphology – cubes and fibers.

To calculate the percolation threshold of the composites, the measurements of electrical conductivity and dielectric constant at 1 kHz for the various rates (matrix / dispersed phase) were carried out.

Figure 13 shows the curves of dielectric constant and conductivity measurements for the CbNN/PVDF composite, where one can observe that there is an abrupt increase in both dielectric constant and conductivity as the ratio is higher than 50% (w/w) for the cubes morphology. Equation 9 jointly with the best linear fit (in the illustrated set) with the value of s = 0.31 +/– 0.08 allow us to indicate that the percolation mechanism (percolation threshold) in this composite and for these processing conditions occur at the rate of 54.6% (w/w). In Figure 13, the threshold value is close to the abrupt increase in conductivity. The composites when subjected to an electric field responded to the field applied accumulating charges on the surface of particles; this charge interferes in the characteristics of the particles–matrix interfaces. The composites formed by the concentrations of morphologically different particles, where the dispersed phase needs different rates (in the matrix phase) so as to occur an interconnection between them. A minimum distance required between the particles prior to the occurrence of percolation is known as interconnection [43]. When the morphology of the particle is in the form of cubes, the distance must be very small in order to promote the contact between them since polarization is homogeneous in the cube–matrix interfaces. Thus, for cubes-like particles a high density of ceramics in the array is required to achieve the interfacial polarization needed to promote the percolation threshold for 54.6% (w/w) of the cubes in the matrix. The variation of dielectric constant and conductivity values prior to the percolation threshold, as can be observed at 40% (w/w), can be linked to the interfacial polarization and the percolation paths in the matrix [44].

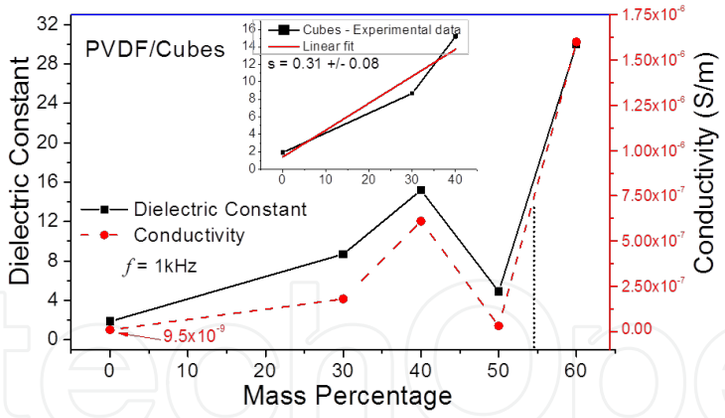

Figure 13. Dielectric constant and conductivity for the various fractions mass of cubes dispersed phase in PVDF matrix. Inset for the best linear fit of the percolation threshold.

The dielectric constant and conductivity values for the FbNN/PVDF composite are illustrated in Figure 14; in this case, there is an abrupt increase in conductivity after 30% (w/w) of fibers. Applying the best linear fit (shown in the inset) with s = 0.90 +/– 0.05 in equation 9 gives you a concentration of 38.0% (w/w) for the percolation threshold. Therefore, the morphology of the fibers, nanoparticles 1D, allows the polarization to reach a long distance over the length of the fiber. A lower concentration of particles enables the interconnection between them so the percolation threshold occurs at only 38% (w/w).

http://dx.doi.org/10.5772/60654

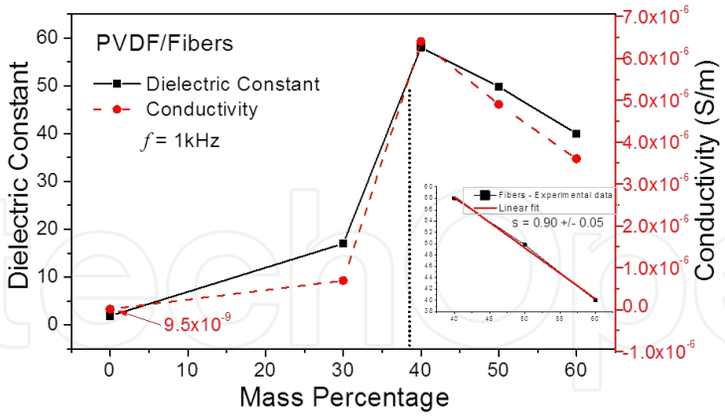

Figure 14. Dielectric constant and conductivity for the various fractions mass of fibers dispersed phase in PVDF matrix. Inset for the best linear fit of the percolation threshold.

Figure 15 presents the data obtained by plotting the dielectric constant and conductivity for the composite FbNN–PAni$_{rep}$/PVDF. The abrupt increase in the dielectric constant and conductivity values is observed from the first analyzed concentration of 30% (w/w). Because of this, it is believed that the percolation threshold is set to a lower concentration. Comparing the three types of dispersed phase of this review, this is the one with the lowest value of percolation threshold, which can be explained by the surface characteristics. The particle morphology 1D indicates a behavior similar to that seen in Figure 14; however, the covering of the fibers with polyaniline which promotes conductivity and the connectivity allowing the percolation threshold is reached with lower concentrations of the dispersed phase. Therefore, to establish the percolation threshold of the composites, a study involving the minor fractions dispersed phase is required. There is also an anomalous behavior observed in Figure 15, for the concentration of 50% (w/w) of dispersed particles. At this point, the results of conductivity and dielectric constant are $1.1x10^{-8}$ and 4.0, respectively. These values are close to those of pure PVDF matrix. This anomalous behavior for the concentrations above the percolation threshold has been observed in some papers that have been published already [41,45,46]. It is suggested that there is a formation of agglomerates with dispersed phase which are found to be isolated functioning as microcapacitors, enveloped by an insulating film that prevents both the load passage and a continued polarization of the network, so a decrease in the dielectric constant and conductivity is verified at this concentration.

The dielectric constant and conductivity values for the dispersed phases and for the pure PVDF are plotted in Figure 16. These values were measured in pellet of these materials. The values of electric conductivity are low contrary to the dielectric constant values which are found to be high. The dielectric constant and conductivity increase in the following order PVDF< cubes< fibers< fibers–PAni$_{rep}$, which can be explained by the fact that this polymer is an insulating material with a rigid structure linked by strong covalent bonds, which can generate a polarization though with difficulty resulting in very low dielectric constant and conductivity. Interestingly, the dispersed phase, which are perovskite oxides, have dipoles in their crystalline structure, making them capable of being oriented quite more easily.

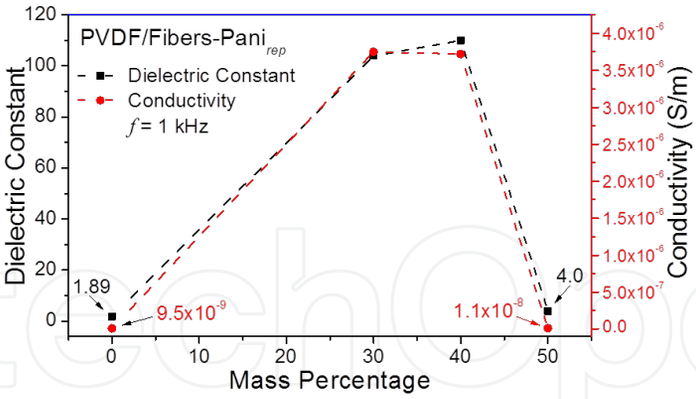

Figure 15. Dielectric constant and conductivity for the various fractions mass of fibers–PAni$_{rep}$ dispersed phase in PVDF matrix. Inset for the best linear fit of the percolation threshold.

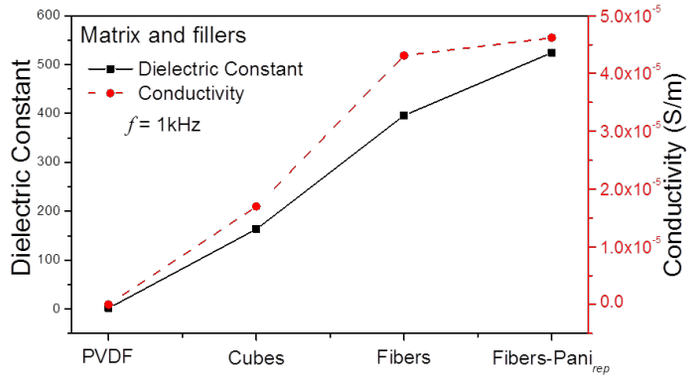

Figure 16. Dielectric constant and conductivity for pure PVDF matrix and the dispersed phase, $NaNbO_3$ with different morphology (cubes, fiber and fiber–PAni$_{rep}$).

The morphology of the dispersed phase directly influences this behavior; the fibers compared with cubes as shown in Figure 16 allow for better charge distribution and thus a higher conductivity. The surface-modified fibers with a conductive polymer, in this case PAni, promote conductivity and permittivity (dielectric constant). The values found for the dielectric constant and conductivity decrease in the order fibers–PAni$_{rep}$, fiber, cubes. The same result is observed for the percolation threshold values, when these materials are used as the dispersed phase in the PVDF matrix, indicating that these factors are interrelated.

4. Conclusion

By microwave hydrothermal synthesis, it is possible to obtain $Na_2Nb_2O_6.nH_2O$ and $NaNbO_3$ orthorhombic crystalline structure particles. The $Na_2Nb_2O_6.nH_2O$ is obtained in fiber-like morphology while $NaNbO_3$ presented cubic-like morphology. The results are associated to synthesis conditions including synthesis time and microwave power. Using 300 W, the increase

http://dx.doi.org/10.5772/60654

in synthesis time favors the formation of $NaNbO_3$; and by 800 and 1000 W the $NaNbO_3$ is obtained within a relatively shorter time. The $Na_2Nb_2O_6.nH_2O$ is used as a precursor to get a fiber-shaped $NaNbO_3$. The thermal treatment of $Na_2Nb_2O_6.nH_2O$ promotes the dehydration and the formation of 1D $NaNbO_3$. The characteristics of the particles exert influence on the material characteristics. Both morphologies of $NaNbO_3$ particles can be mixed with PVDF for the production of flexible composites. An increase in the amount of the ceramics particles leads to the loss of flexibility in the composite owing to the change of connectivity of the ceramic particles and polymer. The anisotropy of ceramic particles improves the composites characteristics, such as $d_{33,}$ Pr, conductivity and dielectric constant values. By inserting a third phase into the composite, these values tend to be higher. The characterization of composite materials indicates the importance of conductivity due to the fact that these materials have multimodal microstructure and each phase has intrinsic properties that determine the properties and applications of the composite formed. These preliminary results demonstrate that the $NaNbO_3$ composite can be used with piezoelectric and ferroelectric properties depending on the material.

Acknowledgements

The authors would like to express their sincerest gratitude and indebtedness to Maximo Siu Li of São Carlos Physical Institute for providing the PL measurements, the LMA-IQ for FEG–SEM facilities and the Brazilian research funding agencies CNPq and FAPESP-CEPID/CDMF 2013/07296-2 for granting the financial support for this research project.

Author details

Guilhermina F. Teixeira[1], Rafael A. Ciola[1], Walter K. Sakamoto[2] and Maria A. Zaghete[1*]

*Address all correspondence to: zaghete@iq.unesp.br

1 Department of Biochemistry and Chemistry Technology, Chemistry Institute, São Paulo State University – UNESP, Araraquara, Brazil

2 Department of Physics and Chemistry, School of Engineering, São Paulo State University, UNESP, Ilha Solteira, Brazil

References

[1] Wu J, Xue D. In situ precursor-template route to semi-ordered $NaNbO_3$ nanobelt arrays. Nanosc Res Lett 2011;6(1):14.

[2] Lue P, Xue D. Growth of one-dimensional MnO2 nanostructure. Mod Phys Lett B 2009;23(31):3835–41.

[3] Schroder DK. Semiconductor Materials and Device Characterization. New York: John Wiley & Sons; 1990.

[4] Wang ZL. Piezopotential gated nanowire devices: piezotronics and piezo-phototronics. Nano Today 2010;5(1):540–52.

[5] Chaiyoa N, Muanghlua R, Niemcharoen S, Boonchom B, Vittayakorn N. Solution combustion synthesis and characterization of lead free piezoelectric sodium niobate ($NaNbO_3$) powders. J Alloy Comp 2011;509(5):2445–9.

[6] Shiratori Y, Magrz A, Ficher W, Pithan C, Waser R. Temperature-induced phase transitions in micro, submicro, and nanocrystalline $NaNbO_3$. J Phys Chem C 2007;111(1): 18493–502.

[7] Boris IK, Oxana VK, Ubaldo OM. Microwave hydrothermal and solvothermal processing of materials and compounds. The development and application of microwave heating. Rijeka: InTech, 2011; pp. 107–40. Available from: http://www.intechopen.com/books/the-development-and-application-of-microwave-heating/microwave-hydrothermal-and-solvothermal-processing-of-materials-and-compounds (accessed 14 January 2015).

[8] Sakamoto WK, Fuzari Jr GC, Zaghete MA, Freitas RLB. Lead titanate-based nanocomposite: fabrication, characterization and application and energy conversion evaluation, Ferroelectrics – material aspects, Rijeka: InTech 2011; pp. 251–77. Available from:http://www.intechopen.com/books/ferroelectrics-material-aspects/lead-titanate-based-nanocomposite-fabrication-characterization-and-application-and-energy-conversion (accessed 14 January 2015).

[9] Skinner DP, Newnham RE, Cross LE. Flexible composite transducers. Mat Res Bull 1978;13(6):599–607.

[10] Newnham RE. Composite electroceramics. Ferroelectrics 1986;68(1):1–32.

[11] Akdogan EK, Allahverdi M, Safari A. Piezoelectric composites for sensor and actuator applications. IEEE Trans Ultrason Ferr 2005;52(5):746–75.

[12] Lee HJ, Zhang S, Bar-Cohen Y, Sherrit S. High temperature, high power piezoelectric composite transducer. Sensors (Basel) 2014;14(8):14526–52.

[13] Seol J-H, Lee JS, Ji H-N, Ok Y-P, Kong GP, Kim K-S, Kim CY, Tai W-P. Piezoelectric and dielectric properties of $(K_{0.44}Na_{0.52}Li_{0.04})(Nb_{0.86}Ta_{0.10}Sb_{0.04})O_3$–PVDF composites. Ceram Int 2012;38(1):S263–6.

[14] Dargahi J. An endoscopic and robotic tooth-like compliance and roughness tactile sensor. J Mech Des 2002;124(3):576–82.

[15] Fuzari Jr G de C, Arlindo EPS, Zaghete MA, Longo E, Sakamoto WK. Poled polyaniline coated piezo composite using low electric field and reduced poling time: a functional material. J Mat Sci Eng B. 2014;4(4):109–15.

[16] Mendoza M, Khan MAR, Shuvo MAI, Guerrero A, Lin Y. Development of lead-free nanowire composites for energy storage applications. ISRN Nanomaterials 2012; doi: 10.5402/2012/151748.

[17] Srinivas K. Possible lead-free nanocomposite polymer dielectrics for high energy storage applications. Int J Adv Eng Nano Technol (IJAENT) 2014;1(9):9–14.

[18] Furukawa T, Ishida K, Fukada E, Piezoelectric properties in the composite systems of polymers and PZT ceramics. J Appl Phys 1979;50(7):4904–12.

[19] Liu XF, Xiong CX, Sun HJ, Dong LJ, Li R, Liu Y. Piezoelectric and dielectric properties of PZT/PVC and graphite doped with PZT/PVC. Compos Mater Sci Eng B Solid State Mater Adv Technol 2006;127(2–3):261–6.

[20] Xu H, Nyman M, Nenoff TM, Navrotsky A. Prototype sandia octahedral molecular sieve (SOMS) $Na_2Nb_2O_6.H_2O$: synthesis, structure and thermodynamic stability. Chem Mater 2004;16(10):2034–40.

[21] Zhu H, Zheng Z, Gao X, Huang Y, Yan Z, Zou J, Yin H, Zou Q, Kable SH, Zhao J, Xi Y, Martens WN, Frost RL. Structural evolution in a hydrothermal reaction between Nb_2O_5 and NaOH solution: from Nb_2O_5 grains to micropourous $Na_2Nb_2O_{6\cdot 2/3}H_2O$ fibers and $NaNbO_3$ cubes. J Am Chem Soc 2006;128(7):2373–84.

[22] Teixeira GF, Wright TR, Manfroi DC, Longo E, Varela JA, Zaghete MA. Photoluminescence in $NaNbO_3$ particles and films. Mater Lett 2015;139(1):443–6.

[23] Wu SY, Liu XQ, Chen XM. Hydrothermal synthesis of $NaNbO_3$ with low NaOH concentration. Ceram Int 2010;36(1):871–7.

[24] Yu A, Liu JQL, Pan H, Zhou X. Surface sprouting growth of $Na_2Nb_2O_6$ H_2O nanowires and fabrication of $NaNbO_3$ nanostructures with controlled morphologies. Appl Surf Sci 2012;258(8):3490–6.

[25] Teixeira GF, Zaghete MA, Varela JA, Longo E. Synthesis and characterization of $NaNbO_3$ mesostructure by a microwave-assisted hydrothermal method. MRS Proc 2014;1675:145–50.

[26] Shi H, Li X, Wang D, Yuan Y, Zou Z, Ye J. $NaNbO_3$ nanostructures: facile synthesis, characterization and their photocatalytic properties. Catal Lett 2009;132(1):205–12.

[27] Ke T-Y, Chen H-A, Sheu H-S, Yeh J-W, Lin H-N, Lee C-Y, Chiu H-T. Sodium niobate nanowire and its piezoelectricity. J Phys Chem C 2008;112(26):8827–31.

[28] Junior ES, La Porta FA, Liu M, Andrés J, Varela JA, Longo E. A relationship among structural, electronic order-disorder effects and optical properties in crystalline TiO_2 nanomaterials. Dalton Trans 2015;44(7):3159–75.

[29] Almeida E, Menezes L de S, Araújo CB de, Lipovskii AA. Luminescence properties and optical dephasing in a glass-ceramic containing sodium-niobate nanocrystals. J Appl Phys 2011;109(11):113108–5.

[30] Teixeira GF, Zaghete MA, Gasparotto G, Costa MGS, Espinosa JWM, Longo E, Varela JA. Photoluminescence properties and synthesis of a PZT mesostructures obtained by the microwave-assisted hydrothermal method. J Alloy Comp 2012;512(1):124–7.

[31] Teixeira GF, Gasparotto G, Paris EC, Zaghete MA, Longo E, Varela JA. Photoluminescence properties of PZT 52/48 synthesized by microwave hydrothermal method using PVA with template. J Lumin 2012;132(1):46–50.

[32] Ribeiro C, Correia DM, Ribeiro S, Sencadas V, Botelho G, Lanceros-Méndez S. Piezoelectric poly(vinylidene fluoride) microstructure and poling state in active tissue engineering. Eng Life Sci 2014;00:1–6.

[33] Marin-Franch P, Martin T, Tunnicliffe DL, Das-Gupta DK. PTCa/PEKK piezo-composites for acoustic emission detection. Sens Actuators A: Physical 2002;99(3):236–43.

[34] Malmonge JA, Malmonge LF, Fuzari Jr GC, Malmonge SM, Sakamoto W.K. Piezo and dielectric properties of PHB–PZT composite. Polym Compos 2009;30(9):1333–7.

[35] Oliveira CA. Otimização do processamento para a obtenção de compósitos polímero/cerâmica com propriedades piezo e piroelétricas. Masters dissertation. UNESP; 2012.

[36] Macario LR. Preparo e caracterização de compósitos polímero/cerâmica com potencial aplicação como sensor multifuncional. PhD thesis. UNESP; 2013.

[37] Pang H, Xu L, Yan DX, Li ZM. Conductive polymer composites with segregated structures. Prog Polym Sci 2014;39(11):1908–33.

[38] Nan C-W. Physics of inhomogeneous inorganic materials. Prog Mater Sci 1993;37(1): 1–116.

[39] Shante VKS, Kirkpatrick S. An introduction to percolation theory. Adv Phys 1971;20(85):325–7.

[40] Dang ZM, Nan CW, Xie D, Zhang YH, Tjong S.C. Dielectric behavior and dependence of percolation threshold on the conductivity of fillers in polymer-semiconductor composites. Appl Phys Lett 2004;85(1):97–9.

[41] Deepa KS, Gopika MS, James J. Influence of matrix conductivity and Coulomb blockade effect on the percolation threshold of insulator-conductor composites. Compos Sci Technol 2013;78(1):18–23.

[42] Deepa KS, Sebastian MT, James J. Effect of interparticle distance and interfacial area on the properties of insulator-conductor composites. Appl Phys Lett 2007:91:202904.

[43] Hong JL, Schadler LS, Siegel RW. Rescaled electrical properties of ZnO/low density polyethylene nanocomposites. Appl Phys Lett 2003;82(12):1956–8.

http://dx.doi.org/10.5772/60654

[44] Tsangaris GM, Psarras GC, Kouloumbi N. Electric modulus and interfacial polarization in composite polymeric systems. J Mater Sci 1998;33(8):2027–37.

[45] Fan P, Wang L, Yang J, Chen F, Zhong M. Graphene/poly(vinylidene fluoride) composites with high dielectric constant and low percolation threshold. Nanotechnol 2012;23(36):365702.

[46] Li Q, Xue Q, Hao L, Gao X, Zheng Q. Large dielectric constant of the chemically functionalized carbon nanotube/polymer composites. Compos Sci Technol 2008;68(10–11):2290–6.

IntechOpen